



TITLE:

Triggering process of whistler mode chorus emissions in the magnetosphere

AUTHOR(S):

Omura, Yoshiharu; Nunn, David

CITATION:

Omura, Yoshiharu ...[et al]. Triggering process of whistler mode chorus emissions in the magnetosphere. Journal of Geophysical Research 2011, 116: A05205.

ISSUE DATE:

2011-06

URL:

<http://hdl.handle.net/2433/141944>

RIGHT:

©2011. American Geophysical Union.; この論文は出版社版ではありません。引用の際には出版社版をご確認ご利用ください。 ; This is not the published version. Please cite only the published version.

1 Triggering process of whistler-mode chorus emissions 2 in the magnetosphere 3

Yoshiharu Omura¹ and David Nunn^{1,2}

4
5 ¹ Research Institute for Sustainable Humanosphere, Kyoto University, Kyoto Japan.
6

7 ² School of Electronics and Computer Science, University of Southampton, Southampton, U.K.
8
9

Yoshiharu Omura, Research Institute for Sustainable Humanosphere, Kyoto University, Uji,
Kyoto, 611-0011, Japan. (omura@rish.kyoto-u.ac.jp)

David Nunn, School of Electronics and Computer Science, University of Southampton,
Southampton, U.K. (dn@ecs.soton.ac.uk)

Chorus emissions are triggered from the linear cyclotron in-

stability driven by the temperature anisotropy of energetic electrons (10 -
100 keV) in the magnetosphere. Chorus emissions grow as an absolute non-
linear instability near the magnetic equator due to the presence of an elec-
tromagnetic electron hole in velocity space. The transition process from the
linear wave growth at a constant frequency to the nonlinear wave growth with
a rising tone frequency is due to formation of a resonant current $-J_B$ anti-
parallel to the wave magnetic field. The rising-tone frequency introduces a
phase shift to the electron hole at the equator, and results in a resonant cur-
rent component anti-parallel to the wave electric field $-J_E$, which causes the
nonlinear wave growth. To confirm this triggering mechanism, we perform
Vlasov Hybrid Simulations with J_B and without J_B . The run without J_B does
not reproduce chorus emissions, while the run with J_B does successfully re-
produce chorus emissions. The nonlinear frequency shift ω_1 due to J_B plays
a critical role in the triggering process. The nonlinear transition time T_N for
the frequency shift is found to be of the same order as the nonlinear trap-
ping period, which is confirmed by simulations and observation. The estab-
lished frequency sweep rate is ω_1/T_N , which gives an optimum wave ampli-
tude of chorus emissions.

1. Introduction

Coherent electromagnetic waves called chorus emissions have frequently been observed in the inner magnetosphere [e.g., *Tsurutani and Smith*, 1974; *Santolik et al.*, 2003; *Santolik*, 2008; *Kasahara et al.*, 2009]. Chorus emissions typically consist of a series of rising tones generated near the magnetic equator, excited by energetic electrons from several keV to tens of keV injected into the inner magnetosphere at the time of a geomagnetic disturbance. In recent years chorus emissions have been studied extensively because of their role as a viable mechanism for accelerating radiation belt electrons as well as precipitating them into the polar atmosphere [*Summers et al.*, 1998; *Summers et al.*, 2002; *Miyoshi et al.*, 2003; *Horne et al.*, 2005; *Omura and Summers*, 2006; *Omura et al.*, 2007; *Katoh and Omura*, 2007; *Furuya et al.*, 2008; *Katoh et al.*, 2008; *Hikishima et al.*, 2010]. As a generation mechanism for chorus emissions, a backward wave oscillator (BWO) theory has been proposed by *Trakhtengerts* [1999]. The BWO theory assumes a step in the velocity distribution function, which has not been observed. Furthermore such a step can only influence the 'triggering phase' and can have no effect upon the plasma dynamics of the established chorus element with sweeping frequency as the resonance velocity will no longer match the location of the step in parallel velocity.

Numerical modeling of chorus emissions have been performed using a Vlasov-Hybrid Simulation (VHS) code based on narrow band field equations derived from Maxwell's equations and the linear equation of motion of cold plasma, under the assumption of a band-limited coherent whistler-mode wave [*Nunn*, 1990, 1993; *Nunn et al.*, 1997, 2009]. The initial wave amplitude and the wave phase are specified in such simulations. In

cast to the VHS code, chorus emissions with rising tones were reproduced successfully

starting from thermal noise in an electromagnetic electron-hybrid code, in which Maxwell's equations are solved directly together with the electron fluid equation for the cold dense electrons and the equations of motion for the hot resonant electrons [Katoh and Omura, 2006; 2007]. The mechanism of the rising chorus emissions has been analyzed theoretically in terms of nonlinear wave growth due to the formation of an electromagnetic electron hole in the velocity phase space [Omura *et al.*, 2008, 2009]. The relation between the wave amplitude and the frequency sweep rate in the generation region of chorus emissions has been derived [Omura *et al.*, 2008, Equation (50)]. The validity of this relation has been demonstrated in a full-particle electromagnetic simulation [Hikishima *et al.*, 2009] as well as in the electron-hybrid simulation [Katoh and Omura, in press]. These simulations show that seeds of chorus emissions with rising tones are formed in a localized region near the magnetic equator. The seeds of emissions grow as a result of the formation of resonant current arising from nonlinear trajectories of resonant untrapped electrons.

Falling tone chorus emissions have also been observed by Cluster spacecraft, and modeled by Nunn *et al.* [2009]. In the present analysis, however, we focus our attention on rising tone chorus emissions, which has been studied more extensively by simulations [Katoh and Omura, 2007; Hikishima *et al.*, 2009; Nunn *et al.*, 2009] as well as observations [Macusova *et al.*, 2010; Cully *et al.*, 2011].

The nonlinear wave growth theory [Omura *et al.*, 2008, 2009] assumed a frequency sweep rate $\partial\omega/\partial t$ that drives the wave growth through the formation of a resonant current J_E parallel to the wave electric field. However, the mechanism for the formation of finite $\partial\omega/\partial t$ has not been clarified yet. Noting that the resonant current J_B parallel to the

magnetic field was included in previous studies based on the VHS code [Nunn *et al.*,

1997, 2009], we have conducted an experiment to run the VHS code with and without J_B to find out the contribution of J_B to the generation of chorus emissions. As shown in Figure 1, the run without J_B does not reproduce a rising tone chorus element, but a constant frequency emission, while the run with J_B does. Considering the contribution of resonant electrons, we first analyze the optimum condition for triggering chorus theoretically in section 2. We confirm the theoretical model by analyzing the result of the Vlasov Hybrid Simulation in section 3. In section 4 we present a summary and discussion.

2. Condition for triggering chorus emissions

We assume a whistler-mode wave propagating parallel to the static magnetic field \mathbf{B}_0 with a wavenumber k and a constant frequency ω_0 satisfying the linear dispersion relation

$$c^2 k^2 - \omega_0^2 - \frac{\omega_0 \omega_{pe}^2}{\Omega_e - \omega_0} = 0 \quad . \quad (1)$$

where c , Ω_e , and ω_{pe} are the speed of light, the electron cyclotron frequency, and the electron plasma frequency, respectively. It is noted that the wavenumber k is a function of a distance h taken along the magnetic field line from the magnetic equator. The wave fields are in the transverse plane containing x - and y -axes. We then assume energetic electrons interacting with the wave satisfying the cyclotron resonance condition

$$\omega_0 - k v_{\parallel} = \frac{\Omega_e}{\gamma} \quad , \quad (2)$$

where γ is the Lorentz factor given by $\gamma = [1 - (v_{\parallel}^2 + v_{\perp}^2)/c^2]^{-1/2}$, and v_{\parallel} and v_{\perp} are electron velocities parallel and perpendicular to \mathbf{B}_0 . Solving for v_{\parallel} , we can obtain an

cit expression of the cyclotron resonance velocity

$$\tilde{V}_R = \frac{\tilde{\omega}^2 - \sqrt{\tilde{\omega}^4 + (\tilde{\omega}^2 + \tilde{V}_p^2)(1 - \tilde{\omega}^2 - \tilde{V}_{\perp 0}^2)}}{\tilde{\omega}^2 + \tilde{V}_p^2} \tilde{V}_p \quad , \quad (3)$$

where $\tilde{\omega} = \omega_0/\Omega_e$, $\tilde{V}_R = V_R/c$, $\tilde{V}_p = V_p/c$, and $\tilde{V}_{\perp 0} = V_{\perp 0}/c$. The phase velocity is given by

$$V_p = \frac{\omega_0}{k_i} = c\delta\xi \quad , \quad (4)$$

where $\xi^2 = \omega_0(\Omega_e - \omega_0)/\omega_{pe}^2$ and $\delta^2 = (1 + \xi^2)^{-1}[Omura et al., 2008]$. When we evaluate γ in the equations derived below, we substitute $v_{\parallel} = V_R$ and $v_{\perp} = V_{\perp 0}$, where $V_{\perp 0}$ is the average perpendicular velocity.

The electrons are organized in phase in the transverse plane, and form a resonant current that can trigger formation of a new wave field with a variable frequency ω , as demonstrated by a full-particle simulation by *Hikishima et al.* [2010].

We express the electric and magnetic field vectors of the total wave field in the transverse plane by the complex forms $\tilde{E}_w = E_w \exp(i\psi_E)$ and $\tilde{B}_w = B_w \exp(i\psi_B)$, respectively. From Maxwell's equations we obtain the following equations for the amplitude B_w of the wave magnetic field in the form [Omura *et al.*, 2008],

$$\frac{\partial B_w}{\partial t} + V_g \frac{\partial B_w}{\partial h} = -\frac{\mu_0 V_g}{2} J_E \quad , \quad (5)$$

$$c^2 k^2 - \omega^2 - \frac{\omega \omega_{pe}^2}{\Omega_e - \omega} = \mu_0 c^2 k \frac{J_B}{B_w} \quad , \quad (6)$$

where μ_0 is the magnetic permittivity in vacuum. The resonant current formed by resonant electrons is divided into two components J_E and J_B parallel to the transverse wave electric and magnetic fields, respectively. Details of the derivation of (5) and (6) are found in Appendix A of *Omura et al.*[2008].

while the resonant current J_E modifies the wave amplitude B_w , the quantity J_B/B_w

changes the frequency ω of the triggered wave. It is noted that the wavenumber k or the wavelength does not change in space and time because it is imposed by the triggering wave with the constant frequency ω_0 in the present situation. Denoting the frequency deviation from ω_0 as ω_1 ($\omega = \omega_0 + \omega_1$) and assuming $\omega_1 \ll \omega_0$, we expand (6) around ω_0 to obtain

$$\left\{ 2\omega_0 + \frac{\Omega_e \omega_{pe}^2}{(\Omega_e - \omega_0)^2} \right\} \omega_1 = -\mu_0 c^2 k \frac{J_B}{B_w} \quad , \quad (7)$$

where we made use of (1). Differentiating (1) with respect to ω_0 , we obtain

$$2c^2k \frac{\partial k}{\partial \omega_0} = 2\omega_0 + \frac{\Omega_e \omega_{pe}^2}{(\Omega_e - \omega_0)^2} \quad . \quad (8)$$

Using (8), we rewrite (7) as

$$\omega_1 = -\frac{\mu_0 V_g}{2} \frac{J_B}{B_w} . \quad (9)$$

where $V_g = \partial\omega_0/\partial k$.

We consider the optimum condition for the nonlinear wave growth to take place, assuming that the electron hole is progressively formed in the velocity phase space within the time window defined by the nonlinear transit time T_N . Dynamics of a resonant electron is described by a set of simplified differential equations. Introducing the variables $\theta = k(v_{\parallel} - V_R)$ and the phase angle ζ between the perpendicular velocity \mathbf{v}_{\perp} and the wave magnetic field \mathbf{B}_w ,

$$\frac{d\zeta}{dt} = \theta \quad , \quad (10)$$

and

$$\frac{d\theta}{dt} = \omega_{tr}^2 (\sin \zeta + S) \quad , \quad (11)$$

$\omega_{tr} = \omega_t \delta \gamma^{-1/2}$, and we have assumed that $\mathbf{v} \sim V_R$, i.e., $\theta \sim 0$. Here, ω_t is the

trapping frequency given by $\omega_t = \sqrt{kv_\perp \Omega_w}$. The shape of the electron hole is determined

by the inhomogeneity ratio given by

$$S = -\frac{1}{s_0\omega\Omega_w}(s_1\frac{\partial\omega}{\partial t} + cs_2\frac{\partial\Omega_e}{\partial h}) \quad , \quad (12)$$

where

$$s_0 = \frac{\delta V_{\perp 0}}{\xi c} \quad , \quad (13)$$

$$s_1 = \gamma \left(1 - \frac{V_R}{V_q}\right)^2, \quad (14)$$

and

$$s_2 = \frac{1}{2\xi\delta} \left\{ \frac{\gamma\omega_0}{\Omega_e} \left(\frac{V_{\perp 0}}{c} \right)^2 - \left[2 + \Lambda \frac{\delta^2(\Omega_e - \gamma\omega_0)}{\Omega_e - \omega_0} \right] \frac{V_R V_p}{c^2} \right\} . \quad (15)$$

We have incorporated the variation of the cold electron density $N_e(h)$ along the magnetic

field line as $N_e(h) = N_{e0}\Omega_e(h)/\Omega_{e0}$, where N_{e0} and Ω_{e0} are respectively the cold electron

density and the electron gyrofrequency at the equator. We have $\Lambda = \omega_0/\Omega_e$ for this

inhomogeneous electron density model, while $\Lambda = 1$ for the constant electron density

model [Omura et al. 2009].

The resonant currents J_E and J_B are expressed respectively as

$$J_E = -J_0 \int_{\zeta_1}^{\zeta_2} [\cos \zeta_1 - \cos \zeta + S(\zeta - \zeta_1)]^{1/2} \sin \zeta d\zeta \quad , \quad (16)$$

and

$$J_B = J_0 \int_{\zeta_1}^{\zeta_2} [\cos \zeta_1 - \cos \zeta + S(\zeta - \zeta_1)]^{1/2} \cos \zeta d\zeta \quad , \quad (17)$$

where $J_0 = (2e)^{3/2}(m_0 k \gamma)^{-1/2} V_{|0}^{5/2} \delta Q G B_w^{1/2}$, and e and m_0 are the charge and rest mass

of an electron. The factor Q represent the depth of the electron hole [Omura *et al.*, 2009].

phase angles ζ_1 and ζ_2 define the boundary of the trapping wave potential as described

by *Omura et al.* [2009]. The parameter G is the value of the velocity distribution function $g(v_{\parallel}, \zeta)$ in the trapping region around the resonance velocity.

We assume that the velocity distribution function f of hot energetic electrons is given in terms of the relativistic momentum per unit mass $u = \gamma v$; u has components $u_{\parallel} = \gamma v_{\parallel}$ and $u_{\perp} = \gamma v_{\perp}$, respectively parallel and perpendicular to the ambient magnetic field. We specify f as

$$f(u_{\parallel}, u_{\perp}) = \frac{N_h}{(2\pi)^{3/2} U_{t\parallel} U_{\perp 0}} \exp\left(-\frac{u_{\parallel}^2}{2U_{t\parallel}^2}\right) \Delta(u_{\perp} - U_{\perp 0}) , \quad (18)$$

where $U_{\perp 0} = \gamma V_{\perp 0}$, $U_{t\parallel}$ is the thermal momentum in the parallel direction, and Δ is the Dirac delta function, and we have normalized f to the density of hot electrons N_h . Integrating over u_{\perp} and taking an average over ζ , we obtain the magnitude G of the unperturbed distribution function $g(v_{\parallel}, \zeta)$ at the resonance velocity V_R as

$$G = \frac{N_h}{(2\pi)^{3/2} U_{t\parallel} U_{\perp 0}} \exp\left(-\frac{\gamma^2 V_R^2}{2U_{t\parallel}^2}\right) . \quad (19)$$

Omura et al. [2008] found that the maximum value of $-J_E$ takes place when $S = -0.413$. Solving (17) for $S = 0.413$, we obtain $J_B = -1.3J_0$, which is rewritten as

$$J_B = -1.3(2e)^{3/2} \left(\frac{B_w}{m_0 k \gamma}\right)^{1/2} V_{\perp 0}^{5/2} \delta Q G . \quad (20)$$

The nonlinear transition time T_N for formation of the nonlinear resonant current is roughly estimated by the nonlinear trapping period T_{tr} given by

$$T_{tr} = \frac{2\pi}{\omega_{tr}} = \frac{2\pi}{\delta} \left(\frac{m_0 \gamma}{k V_{\perp 0} e B_w}\right)^{1/2} , \quad (21)$$

where ω_{tr} is the trapping frequency [*Omura et al.*, 2008]. We define a ratio $\tau = T_N/T_{tr}$, which is to be determined by numerical simulations in the next section.

rough the nonlinear transition time T_N , the electron hole is gradually formed. Along

with formation of J_B , the frequency of the triggered wave gradually deviates from ω_0 to $\omega_0 + \omega_1$. From (9), (19), (20), and (21), we obtain the frequency sweep rate over the nonlinear trapping period as

$$\frac{\omega_1}{T_N} = \frac{1.3}{4} \pi^{-5/2} \frac{Q}{\tau} \left(\frac{\omega_{ph} V_{\perp 0} \delta}{\gamma c} \right)^2 \frac{V_g}{U_{t\parallel}} \exp \left(-\frac{\gamma^2 V_R^2}{2 U_{t\parallel}^2} \right) , \quad (22)$$

where ω_{ph} is the plasma frequency of the hot energetic electrons defined by $\omega_{ph}^2 = \mu_0 c^2 N_h e^2 / m_0$.

At the equator the inhomogeneity of the magnetic field is zero, and the second term on the right-hand side of (12) vanishes. Since the maximum nonlinear wave growth takes place when $S = -0.4$ [Omura *et al.*, 2008], we can derive from (12) the relation between the frequency sweep rate and the normalized wave amplitude at the equator $\Omega_w = e B_w / m_0$ in the form,

$$\frac{\partial \omega}{\partial t} = \frac{0.4 s_0 \omega_0}{s_1} \Omega_w . \quad (23)$$

Equating the left-hand sides of (22) and (23), we obtain an optimum wave amplitude Ω_{wo} that can trigger the rising-tone chorus element as

$$\Omega_{wo} = \frac{s_1 \omega_1}{0.4 s_0 \omega_0 T_N} . \quad (24)$$

From (22) and (24), we obtain

$$\tilde{\Omega}_{wo} = 0.81 \pi^{-5/2} \frac{Q}{\tau} \frac{s_1 \tilde{V}_g}{s_0 \tilde{\omega} \tilde{U}_{t\parallel}} \left(\frac{\tilde{\omega}_{ph} \tilde{V}_{\perp 0} \delta}{\gamma} \right)^2 \exp \left(-\frac{\gamma^2 \tilde{V}_R^2}{2 \tilde{U}_{t\parallel}^2} \right) , \quad (25)$$

where $\tilde{\Omega}_{wo} = \Omega_{wo} / \Omega_{e0}$, $\tilde{\omega}_{ph} = \omega_{ph} / \Omega_{e0}$, and $\tilde{U}_{t\parallel} = U_{t\parallel} / c$.

nally we can evaluate the nonlinear transition time using the wave amplitude obtained

above. Using (4), we rewrite (21) as

$$T_N \Omega_{e0} = 2\pi\tau \left(\frac{\gamma\xi}{\tilde{\omega}\tilde{V}_{\perp 0}\tilde{\Omega}_{w0}\delta} \right)^{1/2}, \quad (26)$$

The triggered chorus element should satisfy another condition to grow as a nonlinear absolute instability at the equator. The wave amplitude of the triggered emission should be greater than the threshold for the nonlinear wave growth [Omura *et al.*, 2009], which is given by

$$\tilde{\Omega}_{th} = \frac{100\pi^3\gamma^3\xi}{\tilde{\omega}\tilde{\omega}_{ph}^4\tilde{V}_{\perp 0}^5\delta^5} \left(\frac{\tilde{a}s_2\tilde{U}_{t\parallel}}{Q} \right)^2 \exp \left(\frac{\gamma^2\tilde{V}_R^2}{\tilde{U}_{t\parallel}^2} \right), \quad (27)$$

where $\tilde{a} = ac^2/\Omega_{e0}^2$, and a is a coefficient defining the parabolic variation of the magnetic field around the equator as $\Omega_e = \Omega_{e0}(1 + ah^2)$. The coefficient a is specified by the L value and the Earth's radius R_E as $a = 4.5/(LR_E)^2$.

3. Simulations of rising tone emissions

We performed simulations of rising tone emissions by the VHS code, in which the equations equivalent to (5) and (6) are solved numerically along with the Vlasov equation for the resonant electrons [Nunn *et al.*, 1990, 1993, 2009]. To find out the importance of the resonant current J_B in generating chorus emissions, we first performed a run in which both J_E and J_B are calculated and the wave field is updated by them. The run produced a rising tone emission as shown in Figure 1(a). We then performed the second run with $J_B = 0$. The second run did not reproduce the rising tone emission as shown in Figure 1(b). A constant frequency emission did result with symmetric upper and lower resonant sidebands. We now recognize the importance of the resonant current J_B as analyzed in the preceding section.

the parameters used in the VHS run are the following. The electron cyclotron frequency

f_c is 8 kHz at the magnetic equator. The electron plasma frequency f_p is 18.8 kHz, which gives $\tilde{\omega}_p = 2.35$. Assuming $L = 4.79$, we have $\tilde{a} = 1.72 \times 10^{-7}$. The velocity distribution assumed in the VHS code is approximated by (18) with $V_{\perp 0} = 0.4584c$, $U_{t\parallel} = 0.2396c$, and $\tilde{\omega}_{ph} = 0.1664$ ($N_h/N_c = 0.005$). These parameter gives equatorial linear growth rate of 600 dB/s, which is in rough agreement with path integrated gain of whistler-mode waves evaluated based on the THEMIS spacecraft observation [Li *et al.*, 2009].

Figures 2(a) and 2(b) show the spatial and temporal variation, in dimensionless units, of wave amplitude B_w/B_0 and wave frequency ω/Ω_{e0} , respectively. The incoming triggering pulse has an initial amplitude $B_{w0} = 4.2 \times 10^{-5}$ (12pT) and duration $8.4 \times 10^3 \Omega_{e0}^{-1}$ (167 ms) and frequency $\omega/\Omega_{e0} = 0.4$ (3.2 kHz). Its amplification as it progresses to the equator is clearly visible in Figure 2a, at which point its amplitude is large enough for nonlinear trapping to occur and for triggering to take place. At about $t\Omega_{e0} \sim 9000$ a riser generation region is firmly established with a wave generation point at the equator and a profile leading edge some $100 \sim 500$ units upstream from the equator.

From the temporal and spatial variation of local frequency in Figure 2(b) we see an initial drop in frequency due to nonlinear trapping in the incoming pulse when it is in the positive inhomogeneity region upstream from the equator $S > 0$. The region of much lower frequencies near $t\Omega_{e0} \sim 8000$ is not significant as it corresponds to very small amplitudes in the wake of the incoming pulse. After $t\Omega_{e0} \sim 9000$ we see a rising frequency in the equatorial region, and after $t\Omega_{e0} \sim 11000$ the progressive establishment of a frequency gradient across the interaction region.

plotting the distribution function of resonant electrons in the $(v_{\parallel} - \zeta)$ phase space,

we find that the depletion of the electrons in the trap at the resonance velocity is about 22 percent of the surrounding energetic electrons. Assuming $Q = 0.25$ with the parameters of the VHS run, we calculated the optimum wave amplitudes given by (25) in solid lines in Figure 3(a). The numbers attached to the lines are the time scale factors τ . We also plot the threshold for the nonlinear wave growth given by (27) in a dashed line. Figure 3(b) shows the nonlinear time scale T_N given by (26) for different values of τ .

In Figure 4 we plot simultaneous time histories at the equator ($h = 0$) of wave amplitude and frequency as well as resonant particle current components J_E and J_B in arbitrary units. Figure 4(a) shows wave amplitude progression. Significant amplitudes $\sim 2 \times 10^{-4}$ are established after $t\Omega_{e0} = 5000$, but there is a drop out around $t\Omega_{e0} \sim 9000$ when the wave profile slips downstream from the equator. Figure 4(b) shows the progression of equatorial frequency. After an initial drop a positive frequency gradient is abruptly established at $t\Omega_{e0} \sim 9000$ of magnitude $1 \times 10^{-5}\Omega_{e0}^2$ (4 kHz/s). From (23), we can estimate the average wave amplitude $B_w/B_{oEQ} = 1.3 \times 10^{-4}$ (37 pT) that results in the frequency sweep rate. Assuming this amplitude is the optimum amplitude given by (25), we find $\tau = 1.0$. Substituting this value of τ into (26), we find $T_N\Omega_{e0} = 640$ (13 ms).

Figure 4(e) shows the time development of the nonlinear frequency shift term ω_1 . The latter is quite interesting. At around $t\Omega_{e0} \sim 9500$ it rises quite quickly to a value ~ 0.006 (50 Hz) which is then sustained. The development time is nearly equal to T_N obtained above. We can also confirm that the quotient ω_1/T_N agrees with the frequency sweep rate $\partial\omega/\partial t = 1 \times 10^{-5}\Omega_{e0}^2$ in accordance with the assumption of the optimum wave amplitude.

a result of trapping in the negative inhomogeneity region $h > 0$, we get an electron

hole and a significant build up of a large nonlinear current J_B at the equator as shown in Figure 4(c). This is as expected since the inhomogeneity S at $h = 0$ is initially zero giving a phase trapping angle anti parallel to the wave magnetic field (phase of 180 degrees relative to B_w). We find formation of a negative J_B around $t\Omega_{e0} = 6500 \sim 8500$, but the wave amplitude is much larger than the optimum wave amplitude, and the nonlinear frequency shift was too small to trigger the rising tone. As the positive frequency sweep rate becomes established at later time as shown in Figure 4(b), S shifts to a value ~ -0.4 which enables us to easily interpret the J_E profile in Figure 4(d). The current J_E is initially close to zero as expected for $S = 0$, but acquires a significant negative component, from about $t\Omega_{e0} \sim 9500$ giving nonlinear growth, as the trapping angle rotates to a phase of approximately 166 degrees.

We performed a few other runs of rising chorus elements by the VHS code with different parameters, and found the same sequence of the initial formation of the negative J_B followed by gradual formation of the negative J_E along with establishment of the finite frequency sweep rate. We also found $\tau \sim 1.0$.

In Figure 5(a) we plot the optimum wave amplitude and the threshold for the nonlinear wave growth with parameters used in an electron hybrid simulation [Kato and Omura [2007]: Omura *et al.*, 2008] $\tilde{a} = 9.8 \times 10^{-7}$, $\tilde{V}_{\perp 0} = 0.6$, $\tilde{U}_{t\parallel} = 0.3$, $\tilde{\omega}_{pe} = 4$, and $\tilde{\omega}_{ph} = 0.113$. We assume $Q = 0.5$ and different values of $\tau = 0.25, 0.5, 1.0, 2.0$. Noting that the simulated chorus emissions have frequency spectra starting from $\omega = 0.2\Omega_{e0}$ with the wave amplitude $B_w \sim 4 \times 10^{-4} B_{0EQ}$ at the equator (Figures 4 and 5 of Omura *et al.* [2008]), we find that the optimum amplitude with $\tau = 0.25 \sim 0.5$ agrees with the simulation result, because

frequency range above $\omega = 0.2$ satisfies the necessary condition for the nonlinear wave

growth $\tilde{\Omega}_{wo} > \tilde{\Omega}_{th}$.

In Figure 5(b), we plot the optimum wave amplitude and the threshold with parameters used in a full-particle simulation by *Hikishima et al.*[2009]: $\tilde{a} = 5.1 \times 10^{-6}$, $\tilde{V}_{\perp 0} = 0.29$, $\tilde{U}_{t\parallel} = 0.2$, $\tilde{\omega}_{pe} = 5$, and $\tilde{\omega}_{ph} = 0.40$. In both cases, we assume $Q = 0.5$ and different values of $\tau = 0.25, 0.5, 1.0, 2.0$. Figure 8 of *Hikishima et al.* [2009] shows chorus emissions starting from $\omega = 0.16\Omega_{e0}$ with a wave amplitude $B_w \sim 1 \times 10^{-3}B_{0EQ}$ at the equator. We find good agreement between the optimum amplitude with $\tau = 0.5$ and the frequency spectra of the simulation result.

It is also interesting to note that the frequency range that satisfies $\tilde{\Omega}_{wo} > \tilde{\Omega}_{th}$, shown in Figure 5(a), agrees with the width of the wave spectra found in the simulation result. A chorus element undergoes a strong wave amplitude modulation through its evolution in frequency. Even if the nonlinear wave growth is terminated because of the amplitude modulation, a new triggering process can take place when the optimum condition of the wave amplitude is satisfied, and the rising tone is resumed. Therefore, while the optimum wave amplitude is larger than the threshold for the nonlinear wave growth, the frequency continues to increase, forming the chorus element.

4. Summary and Discussion

We have obtained an optimum wave amplitude that can trigger a rising tone chorus element. When the optimum wave amplitude given by (25) is reached by the linear wave instability at a specific frequency driven by the temperature anisotropy of resonant electrons near the equator, a triggered emission arises with a rising frequency due to gradual formation of the negative J_B and with an increasing wave amplitude due to the

positive J_E induced by the positive frequency sweep rate. An electromagnetic electron

hole is formed in the velocity phase space with $S \sim -0.4$. An absolute nonlinear instability takes place above the threshold given by (27).

For comparison with an observation by the Cluster spacecraft [*Santolik et al.*, 2003; *Santolik*, 2008], we plot the optimum wave amplitude and the threshold for the nonlinear wave growth in Figure 6(a), and the theoretical frequency sweep rate $\partial f/\partial t$ in Figure 6(b). Based on the observation at $L = 4.4$, which gives $\tilde{a} = 2 \times 10^{-7}$, we assumed parameters as $\omega_{pe}/\Omega_{e0} = 2.4$, $\tilde{V}_{\perp 0} = 0.3$, and $\tilde{U}_{t\parallel} = 0.2$. The energy of the resonant electrons are 50 keV for $\omega/\Omega_{e0} = 0.37$ (3 kHz). Since the parameters are very close to the VHS run, we use $Q = 0.25$ and varied the time scale parameter as $\tau = 0.25, 0.5, 1.0, 2.0$. The optimum wave amplitude and the frequency sweep rate varies depending on the density of energetic electrons N_h . From the observation, we can find the frequency sweep rates, which do not change much through propagation. On the other hand, the wave amplitude can change substantially through propagation from the source region to the observation point. Therefore, we can infer the physical parameters at the generation region from the frequency sweep rate of the observed chorus emissions. Chorus emissions reported by *Santolik et al.*[2003] consist of rising tone elements starting from 2 ~ 3 kHz with the frequency sweep rate ~ 15 kHz/s. We find a good agreement with the case $N_h/N_c = 0.04$ and $\tau = 0.25 \sim 0.5$. The wave amplitude in the generation region is estimated as large as 100 ~ 300 pT.

It is also interesting to note that the frequency sweep rate give by (22) does not depend on the wave amplitude of the triggering wave. The physical plasma parameters and the frequency of the triggering wave determine the frequency sweep rate. Then the effective

growth takes place with the wave amplitude of the triggered wave, which satisfies

the condition (23) at the magnetic equator.

Finally we can construct the following scenario of the chorus generation process, summarizing the recent studies [Omura *et al.*, 2008, 2009] and the present analysis.

1. Linear Phase: Whistler-mode waves grow due to a linear instability driven by temperature anisotropy of energetic electrons. A constant-frequency wave with the maximum linear growth rate becomes dominant to form a coherent wave phase. The linear growth rate maximizes at the magnetic equator where the flux of energetic electrons at the resonance velocity becomes largest. The seed of the triggering wave is the thermal fluctuation at some distance from the equator. It propagates toward the equatorial region, undergoing the convective linear growth to form a coherent wave near the equator.

2. Nonlinear Phase 1: As a result of the nonlinear dynamics of electrons at or near the resonance velocity of the triggering coherent wave, a hole in the velocity distribution function at the location of the resonant particle trap is formed. The negative resonant current J_B is formed, resulting in the nonlinear frequency shift ω_1 taking place over T_N , which is of the same order as the nonlinear trapping time T_{tr} . The ratio T_N/T_{tr} ($= \tau$) is $0.25 \sim 1.0$. The frequency sweep rate is the nonlinear frequency shift ω_1 divided by the nonlinear transition time T_N .

3. Nonlinear Phase 2: Along with the establishment of the frequency sweep rate ω_1/T_N , the nonlinear resonant current J_E is formed, resulting in the nonlinear wave growth. Formation of the negative J_E results in the nonlinear wave growth as an absolute instability at the magnetic equator. The nonlinear instability starts from an optimum amplitude that is required to maximize J_E with the inhomogeneity ratio $S = -0.4$. The

the evolution of the wave amplitude and frequency is described by the chorus equations

[*Omura et al.*, 2009].

4. Nonlinear Phase 3: A chorus element is formed at the magnetic equator, and propagates away from it. As the wave propagates away from the equator, the zero order field gradient increases as does the wave amplitude due to the nonlinear wave growth. While $-1 < S < 0$, trapping is allowed and the chorus element continues to grow as it propagates away from the equator.

In the linear phase, the triggering wave grows from the thermal fluctuation through the convective linear growth. Evaluation of the path-integrated gain of the linear instability was performed by *Li et al.* [2009]. It is noted, however, that the linear growth rate is applicable only to the triggering waves, and not to the chorus emissions, which are generated through the nonlinear processes as described above.

The initial appearance of J_B followed by J_E in the initial nonlinear growth phase of the triggered emissions is also observed in the HAARP HF ionospheric heating experiment [*Golkowski et al.*, 2010]. From the growth of the observed wave amplitudes and phases of HAARP-generated whistler-mode echoes, the magnitudes of the resonant currents are estimated. The analysis shows that the magnitude of J_B is greater than that of J_E , which is consistent with the VHS code result shown in Figure 4 and the theoretical model of an electromagnetic electron hole assumed in the nonlinear wave growth theory.

Gibby et al. [2008] tried to reproduce triggered emissions, using a more classical Vlasov method such as developed by *Denavit* [1972; 1985] and by *Besse and Sonnendrucker* [2003] in the semi Lagrangian method. These methods advance the distribution function by applying Liouville's theorem to one step particle trajectories, and then interpolating

distribution function back onto the phase space grid. These methods can have poor

robustness to distribution function filamentation and give rise to an unphysical diffusion in distribution function due to the successive interpolation procedures. The VHS method suffers from neither of these problems. The code by *Gibby et al.* [2008] does not update wave phase properly when wave amplitude is very small and for a broadband simulation has a rather low resolution in phase space, which may be why the code does not trigger emissions. *Gibby et al.* [2008] presents interesting and plausible data, supported by his simulations, suggesting that in the key down case saturation may arise from marked spectral broadening which destroys particle trapping and thus nonlinear growth rates.

At the magnetic equator, the nonlinear wave growth saturates due to a subsequent nonlinear effect [*Hikishima et al.*, 2010]. The detailed analysis of the saturation mechanism is left as a future study.

Acknowledgments. Computation in the present study was performed with the KDK system of Research Institute for Sustainable Humanosphere (RISH) at Kyoto University. This work was supported by Grant-in-Aid 20340135 of the Ministry of Education, Science, Sports and Culture of Japan. D. Nunn thanks Kyoto University for Visiting Professorship at RISH.

References

- Besse, N. and E. Sonnendruker (2003), Semi-Lagrangian schemes for the Vlasov Equation on an Unstructured Mesh of Phase Space, *J. Computational Physics*, 191, no 2, 341-376.
- Cully, C. M., V. Angelopoulos, U. Auster, J. Bonnell, and O. Le Contel (2011), Observational evidence of the generation mechanism for rising tone chorus, *Geophys. Res.*

Denavit, J. (1972), Numerical Simulation of Plasmas with Periodic Smoothing in Phase Space, *J. Computational Physics*, 9, 75-98.

Denavit, J. (1985), Simulations of Bump-on-Tail Instability, *Physics of Fluids*, 28 (9), 2773-2777.

Gibby, A. R., U. S. Inan, and T. F. Bell (2008), Saturation effects in the VLF-triggered emission process, *J. Geophys. Res.*, 113, A11215, doi:10.1029/2008JA013233.

Golkowski, M., U. S. Inan, M. B. Cohen, and A. R. Gibby (2010), Amplitude and phase of nonlinear magnetospheric wave growth excited by the HAARP HF heater, *J. Geophys. Res.*, 115, A00F04, doi:10.1029/2009JA014610.

Hikishima, M., Y. Omura, D. Summers, Self-consistent particle simulation of whistler-mode triggered emissions, *J. Geophys. Res.*, 115, A12246, doi:10.1029/2010JA015860.

Hikishima, M., S. Yagitani, Y. Omura, and I. Nagano (2009), Full particle simulation of whistler-mode rising chorus emissions in the magnetosphere, *J. Geophys. Res.*, 114, A01203, doi:10.1029/2008JA013625.

Hikishima, M., Y. Omura, and D. Summers (2010), Microburst precipitation of energetic electrons associated with chorus wave generation, *Geophys. Res. Lett.*, 37, L07103, doi:10.1029/2010GL042678.

Horne, R. B., R. M. Thorne, S. A. Glauert, J. M. Albert, N. P. Meredith, and R. R. Anderson (2005), Timescale for radiation belt electron acceleration by whistler mode chorus waves, *J. Geophys. Res.*, 110, A03225, doi: 10.1029/2004JA00811.

Kasahara, Y., Y. Miyoshi, Y. Omura, O. P. Verkhoglyadova, I. Nagano, I. Kimura, and B. T. Tsurutani (2009), Simultaneous satellite observations of VLF chorus, hot and

ativistic electrons in a magnetic storm recovery phase, *Geophys. Res. Lett.*, *36*,

L01106, doi:10.1029/2008GL036454.

Katoh, Y. and Y. Omura (2006), A study of generation mechanism of VLF triggered emission by self-consistent particle code, *J. Geophys. Res.*, *111*, A12207, doi:10.1029/2006JA011704.

Katoh, Y. and Y. Omura (2007), Computer simulation of chorus wave generation in the Earth's inner magnetosphere, *Geophys. Res. Lett.*, *34*, L03102, doi:10.1029/2006GL028594.

Katoh, Y. and Y. Omura, Amplitude dependence of frequency sweep rates of whistler-mode chorus emissions, *J. Geophys. Res.*, doi:10.1029/2010JA016058, in press.

Katoh, Y., Y. Omura, and D. Summers (2008), Rapid energization of radiation belt electrons by nonlinear wave trapping, *Ann. Geophys.*, *26*, 3451.

Li, W., R. M. Thorne, V. Angelopoulos, J. W. Bonnell, J. P. McFadden, C. W. Carlson, O. LeContel, A. Roux, K. H. Glassmeier, and H. U. Auster (2009), Evaluation of whistler-mode chorus intensification on the nightside during an injection event observed on the THEMIS spacecraft, *J. Geophys. Res.*, *114*, A00C14, doi:10.1029/2008JA013554.

Macusova, E., O. Santolik, P. Decreau, A. G. Demekhov, D. Nunn, D. A. Gurnett, J. S. Pickett, E. E. Titova, B. V. Kozelov, J. L. Rauch, and J. G. Trotignon (2010), Observations of the relationship between frequency sweep rates of chorus wave packets and plasma density, *J. Geophys. Res.*, *115*, A12257, doi:10.1029/2010JA015468.

Miyoshi, Y., A. Morioka, T. Obara, H. Misawa, T. Nagai, and Y. Kasahara (2003), Rebuilding process of the outer radiation belt during the 3 November 1993 magnetic storm: NOAA and Exos-D observations, *J. Geophys. Res.*, *108* (A1), 1004, doi:

Nunn, D., Y. Omura, H. Matsumoto, I. Nagano, and S. Yagitani (1997), The numerical simulation of VLF chorus and discrete emissions observed on the Geotail satellite using a Vlasov code, *J. Geophys. Res.*, *102*, 27083.

Nunn, D., O. Santolik, M. Rycroft, and V. Trakhtengerts (2009), On the numerical modelling of VLF chorus dynamical spectra, *Ann. Geophys.*, *27*, 2341.

Nunn, D. (1990), The numerical simulation of non linear VLF wave particle interactions using the Vlasov Hybrid Simulation technique, *Computer Physics Comms.*, *60*, pp 1-25.

Nunn, D. (1993), Vlasov Hybrid Simulation - A novel method for the numerical simulation of hot collision free plasmas, *Journal of Computational Physics*, *108*, *1*, pp180-196.

Omura, Y., and H. Matsumoto (1982), Computer simulations of basic processes of coherent whistler wave-particle interactions in the magnetosphere, *J. Geophys. Res.*, *87*, 4435.

Omura, Y., and D. Summers (2006), Dynamics of high-energy electrons interacting with whistler mode chorus emissions in the magnetosphere, *J. Geophys. Res.*, *111*, A09222, doi:10.1029/2006JA011600.

Omura, Y., N. Furuya, and D. Summers (2007), Relativistic turning acceleration of resonant electrons by coherent whistler mode waves in a dipole magnetic field, *J. Geophys. Res.*, *112*, A06236, doi:10.1029/2006JA012243.

Omura, Y., Y. Katoh, and D. Summers (2008), Theory and simulation of the generation of whistler-mode chorus, *J. Geophys. Res.*, *113*, A04223, doi:10.1029/2007JA012622.

Omura, Y., M. Hikishima, Y. Katoh, D. Summers, and S. Yagitani (2009), Nonlinear mechanisms of lower-band and upper-band VLF chorus emissions in the magnetosphere,

493 Santolik, O., D. A. Gurnett, and J. S. Pickett, Multipoint investigation of the source
494 region of storm-time chorus (2004), *Ann. Geophys.*, 22,2255.

495 Santolik, O., D. A. Gurnett, J. S. Pickett, M. Parrot, and N. Cornilleau-Wehrlin (2003),
496 Spatio-temporal structure of storm-time chorus, *J. Geophys. Res.*, 108 (A7), 1278,
497 doi:10.1029/2002JA00979

498 Santolik, O. (2008), New results of investigations of whistler-mode chorus emissions, *Non-*
499 *lin. Processes Geophys.*, 15, 621.

500 Summers, D., R. M. Thorne, and F. Xiao (1998), Relativistic theory of wave-particle
501 resonant diffusion with application to electron acceleration in the magnetosphere, *J.*
502 *Geophys. Res.*, 103, 20487.

503 Summers, D., C. Ma, N. P. Meredith, R. B. Horne, R. M. Thorne, D. Heynderickx, and
504 R. R. Anderson (2002), Model of the energization of outer-zone electrons by whistler-
505 mode chorus during the October 9, 1990 geomagnetic storm, *Geophys. Res. Lett.*, 29
506 (4), 2174, doi: 10.1029/2002GL016039.

507 Trakhtengerts, V. Y. (1999), A generation mechanism for chorus emission, *Anal. Geo-*
508 *physicae*, 17, 95.

509 Tsurutani, B. T., and E. J. Smith (1974), Postmidnight chorus: A substorm phenomenon,
510 *J. Geophys. Res.*, 79, 118.

Figure 1. Dynamic spectra of VHS code runs (a) with J_B and (b) without J_B .

Figure 2. Spatial and temporal evolutions of (a) wave amplitude and (b) frequency in the VHS code run with J_B . The dashed white lines indicate the time when the formation of the nonlinear current J_B begins. The arrow in magenta indicates the wave packet of the triggering wave.

Figure 3. (a) The optimum wave amplitudes (solid lines) for triggering rising tone emissions with different values of the time scale factor τ (attached numbers), and the threshold of the wave amplitude for the nonlinear wave growth (dashed line) with the parameters used in the VHS run. (b) The corresponding nonlinear transition time T_N for formation of the nonlinear resonant current $-J_B$ with different values of the time scale factor τ .

Figure 4. Time histories of the wave amplitude, frequency, resonant currents J_B and J_E , and nonlinear frequency shift ω_1 at the magnetic equator in the VHS code run. The dashed blue lines indicates the time when the formation of $-J_B$ begins, and the dashed red line indicates the time when $-J_E$ is formed, resulting in the nonlinear wave growth.

Figure 5. The optimum wave amplitudes (solid lines) with different values of τ (attached numbers) and the threshold for nonlinear wave growth (dashed line), (a) for simulation parameters used in *Katoh and Omura* [2007], and (b) for simulation parameters used in *Hikishima et al.* [2009].

Figure 6. (a) The optimum wave amplitudes for rising tone emissions (solid lines) with different values of τ (attached numbers), and the threshold of wave amplitude for the nonlinear wave growth (dashed line) and (b) the corresponding frequency sweep rates with the energetic electron density $N_h/N_c = 0.04$. Other physical parameters are specified for an observation by the Cluster spacecraft [*Santolik et al.*, 2003; *Santolik*, 2008].

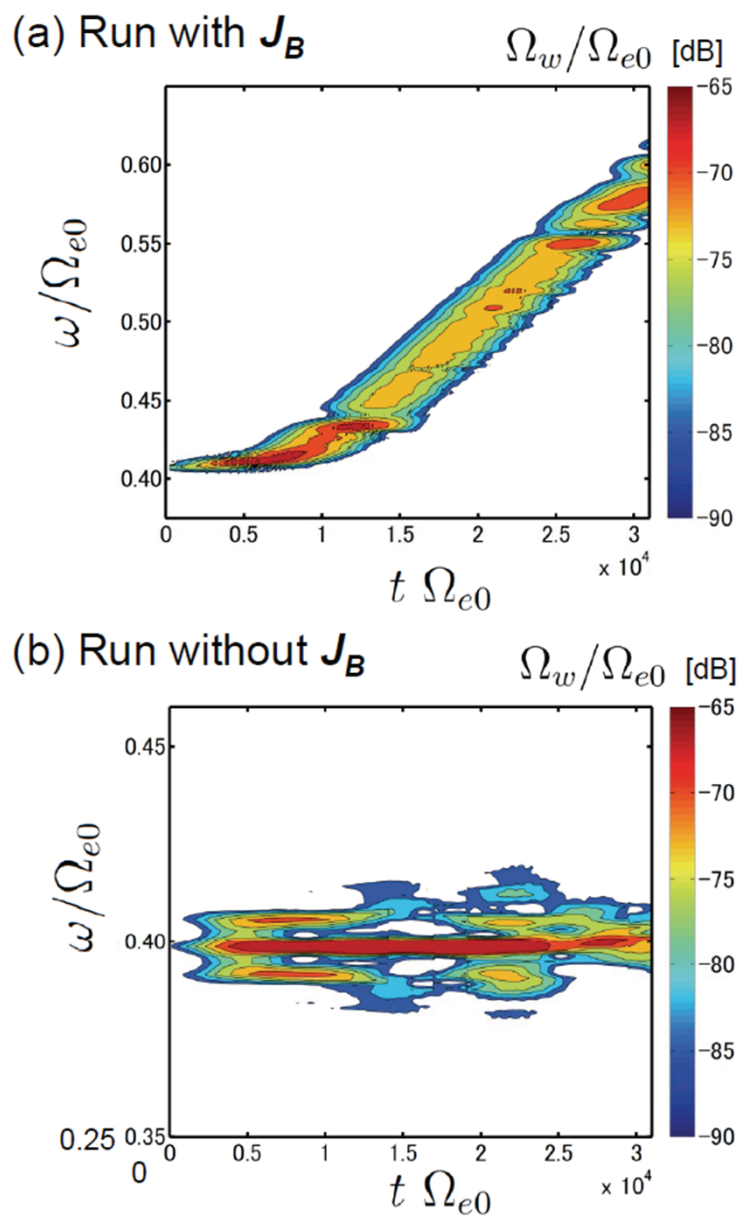


Figure 1. Dynamic spectra of VHS code runs (a) with J_B and (b) without J_B .

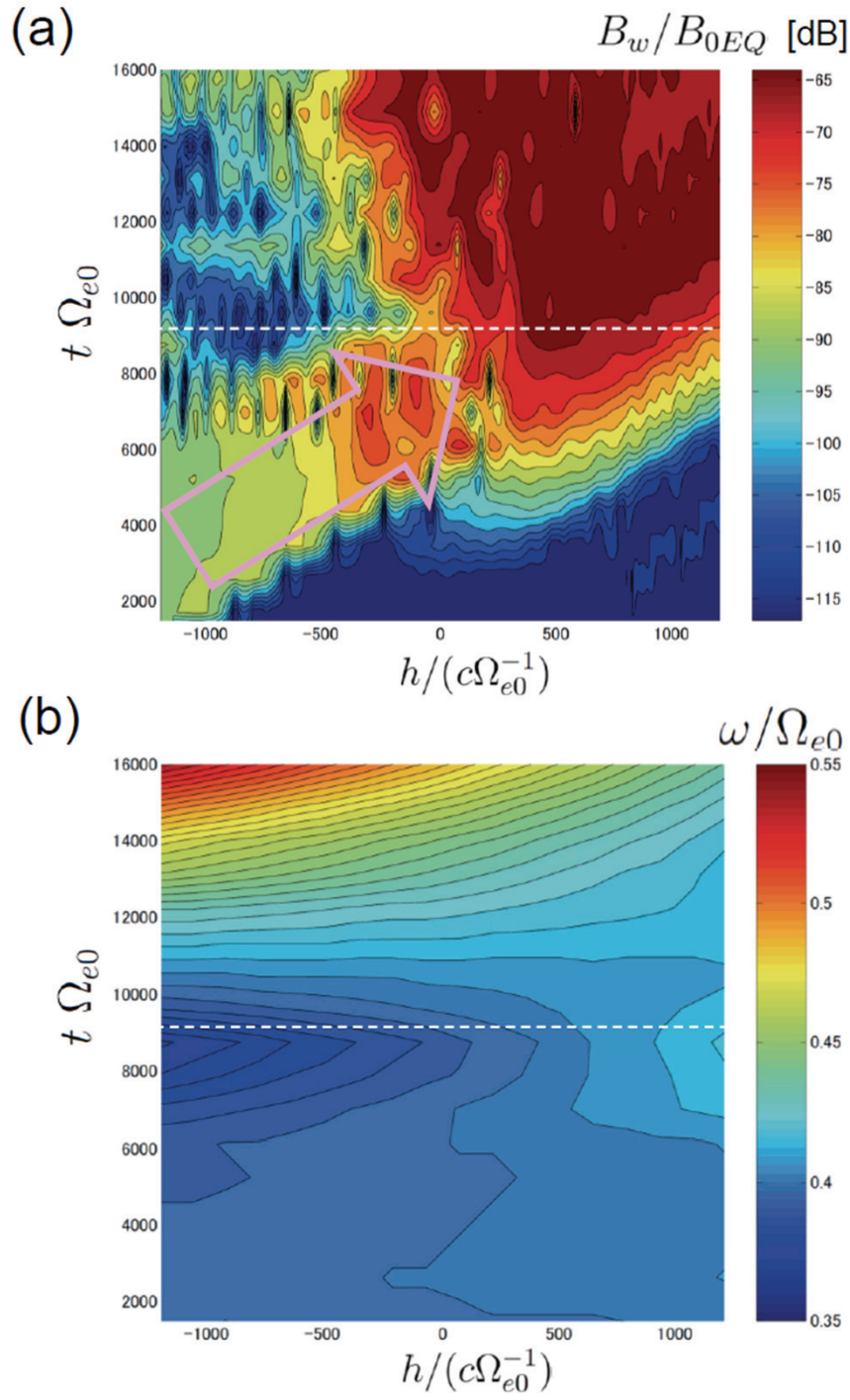


Figure 2. Spatial and temporal evolutions of (a) wave amplitude and (b) frequency in the VHS code run with J_B . The dashed white lines indicate the time when the formation of the nonlinear current J_B begins. The arrow in magenta indicates the wave packet of the triggering wave.

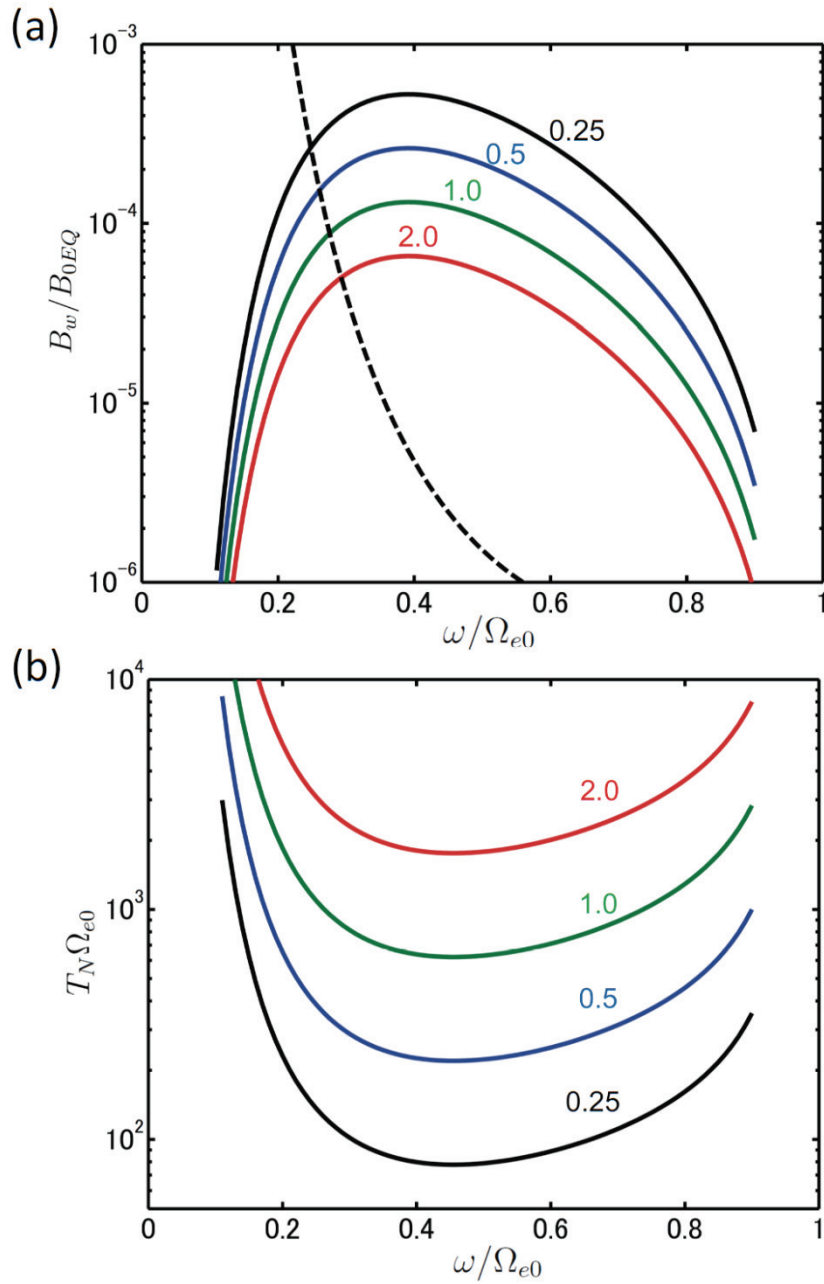


Figure 3. (a) The optimum wave amplitudes (solid lines) for triggering rising tone emissions with different values of the time scale factor τ (attached numbers), and the threshold of the wave amplitude for the nonlinear wave growth (dashed line) with the parameters used in the VHS run. (b) The corresponding nonlinear transition time T_N for formation of the nonlinear resonant current $-J_B$ with different values of the time scale factor τ .

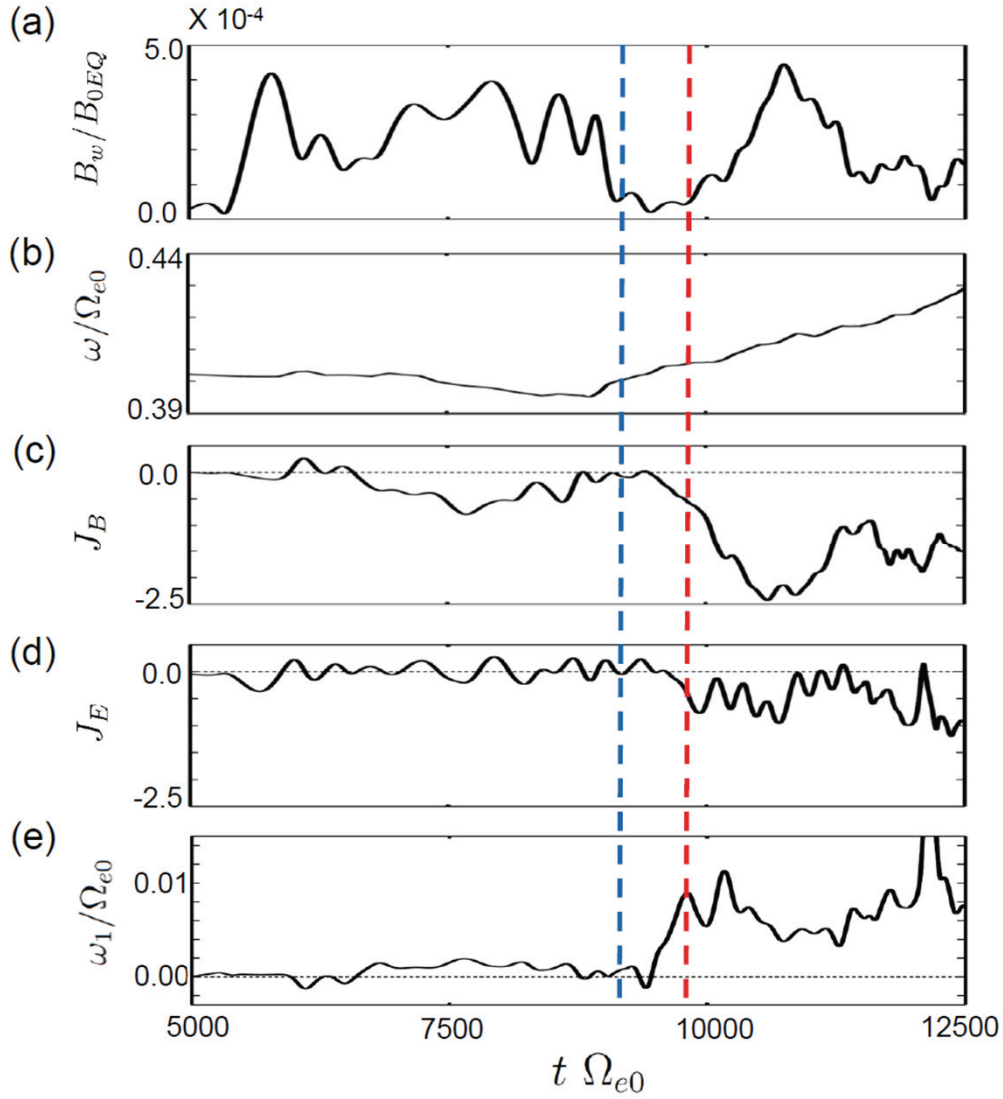


Figure 4. Time histories of the wave amplitude, frequency, resonant currents J_B and J_E , and nonlinear frequency shift ω_1 at the magnetic equator in the VHS code run. The dashed blue lines indicates the time when the formation of $-J_B$ begins, and the dashed red line indicates the time when $-J_E$ is formed, resulting in the nonlinear wave growth.

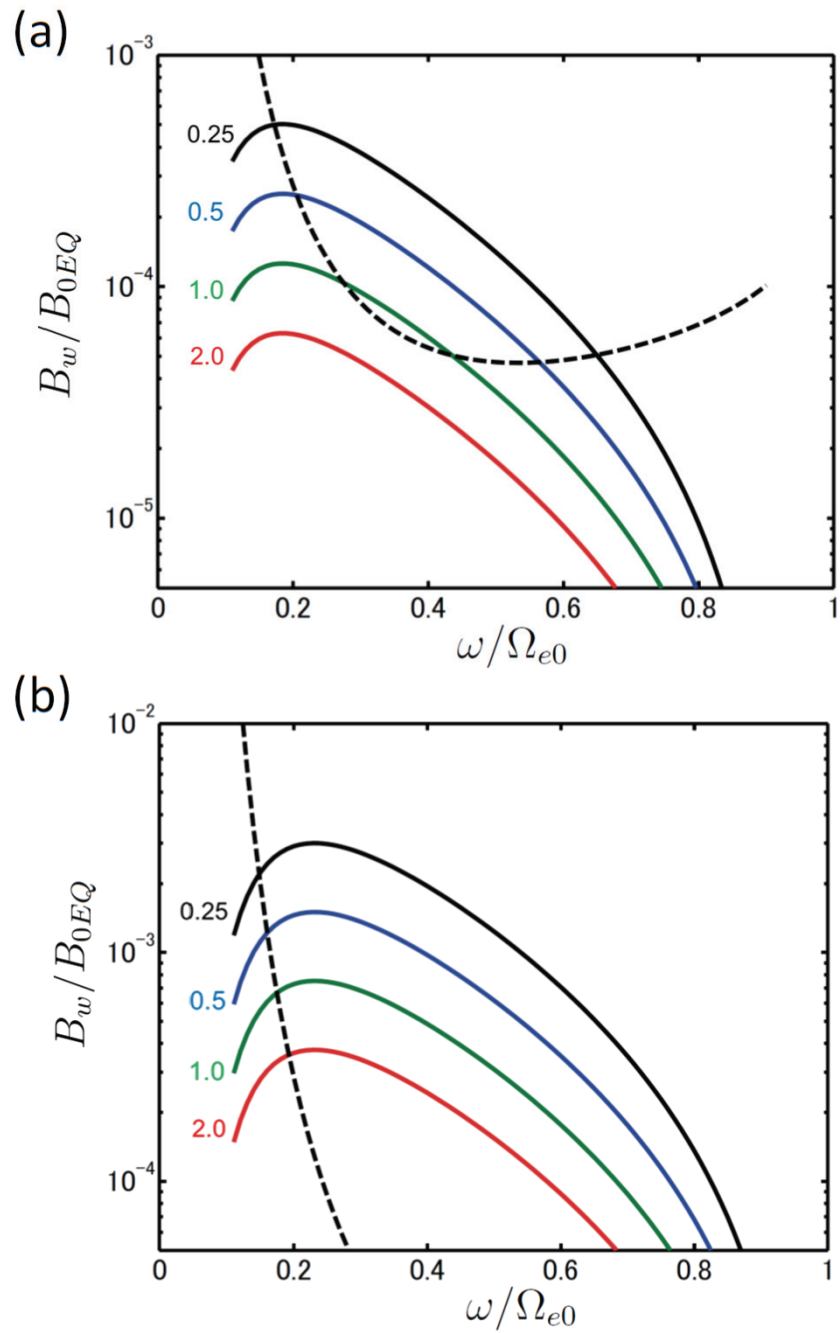


Figure 5. The optimum wave amplitudes (solid lines) with different values of τ (attached numbers) and the threshold for nonlinear wave growth (dashed line), (a) for simulation parameters used in *Katoh and Omura [2007]*, and (b) for simulation parameters used in *Hikishima et al. [2009]*.

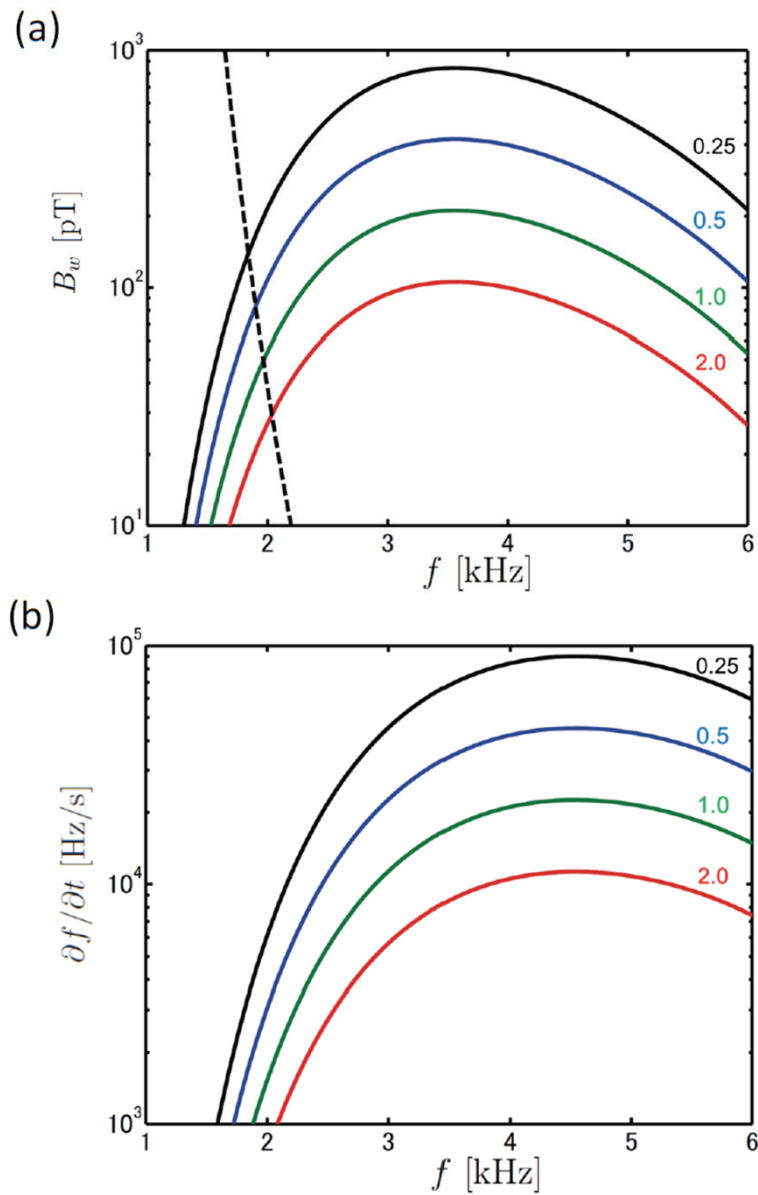


Figure 6. (a) The optimum wave amplitudes for rising tone emissions (solid lines) with different values of τ (attached numbers), and the threshold of wave amplitude for the nonlinear wave growth (dashed line) and (b) the corresponding frequency sweep rates with the energetic electron density $N_h/N_c = 0.04$. Other physical parameters are specified for an observation by the Cluster spacecraft [Santolik *et al.*, 2003; Santolik, 2008].